Giant Planet Formation by Disk Instability in Low Mass Disks?

Alan P. Boss

Department of Terrestrial Magnetism, Carnegie Institution of Washington, 5241 Broad Branch Road, NW, Washington, DC 20015-1305

boss@dtm.ciw.edu

ABSTRACT

Forming giant planets by disk instability requires a gaseous disk that is massive enough to become gravitationally unstable and able to cool fast enough for self-gravitating clumps to form and survive. Models with simplified disk cooling have shown the critical importance of the ratio of the cooling to the orbital timescales. Uncertainties about the proper value of this ratio can be sidestepped by including radiative transfer. Three-dimensional radiative hydrodynamics models of a disk with a mass of $0.043 M_\odot$ from 4 to 20 AU in orbit around a $1 M_\odot$ protostar show that disk instabilities are considerably less successful in producing self-gravitating clumps than in a disk with twice this mass. The results are sensitive to the assumed initial outer disk (T_o) temperatures. Models with $T_o = 20$ K are able to form a single self-gravitating clump, whereas models with $T_o = 25$ K form clumps that are not quite self-gravitating. These models imply that disk instability requires a disk with a mass of at least $\sim 0.043 M_\odot$ inside 20 AU in order to form giant planets around solar-mass protostars with realistic disk cooling rates and outer disk temperatures. Lower mass disks around solar-mass protostars must rely upon core accretion to form inner giant planets.

Subject headings: accretion, accretion disks — hydrodynamics — instabilities — planets and satellites: formation — solar system: formation

1. Introduction

The emerging census of extrasolar planets has revealed an abundance of exoplanets, ranging from super-Earths to super-Jupiters. Mayor et al. (2009) suggest that $\sim 30\%$ of solar-type stars have short period (less than 100 days) super-Earths with masses less than 30 $M_\oplus$. The estimated frequency of giant planets with masses in the range from 0.3 to 10 M_J (Jupiter-masses) inside ~ 20 AU is $\sim 10\%$ to $\sim 20\%$ (Cumming et al. 2008). Gravitational

microlensing detections imply an even higher frequency of giant planets orbiting beyond 3 AU, about 35% (Gould et al. 2010). Giant planet formation thus appears to be a reasonably common outcome of the low-mass star formation process.

While core accretion continues to be the most popular mechanism for giant planet formation (e.g., Johnson et al. 2010), disk instability seems to be necessary as well, at least in order to explain the formation of gas giant planets orbiting at great distances. HR 8799, e.g., appears to have a system of three giant planets, orbiting at distances of 24, 38, and 68 AU, with masses of 10, 10, and 7 M_J, respectively (Marois et al. 2008). Core accretion appears to be unable to form gas giants beyond ~ 35 AU even in the most favorable circumstances (e.g., Levison & Stewart 2001; Thommes, Duncan, & Levison 2002; Chambers 2006), and gravitational scattering outward of planets formed closer in does not seem to lead to stable wide orbits (Dodson-Robinson et al. 2009; Raymond, Armitage, & Gorelick 2010). Disk instability appears to be the more likely mechanism for forming wide gas giant planets (Boss 2003, 2010; Dodson-Robinson et al. 2009; Boley 2009), while its utility for forming planets much closer in continues to be debated (e.g., Boss 2009).

At a minimum, the disk instability mechanism require two conditions to be met in order to produce giant planets: a disk sufficiently massive and cold enough to be gravitationally unstable, and the ability to radiate away enough energy produced by compressional heating to allow any clumps that form to contract toward planetary densities (e.g., Helled, Podolak, & Kovetz 2006; Helled & Bodenheimer 2010). The latter question has been a particular focus of study, with much effort devoted to simplified models where disk cooling occurs over a timescale t_{cool}. Gammie (2001) found that fragmentation should occur in two dimensional (razor-thin) disks with $\beta \leq \beta_{crit} \sim 3$, where $\beta = t_{cool}\Omega$, with Ω being the disk's angular frequency. Rice et al. (2003) found that $\beta_{crit} \sim 6$ led to fragmentation in their three dimensional disk simulations. Boss (2004) estimated that $\beta \sim 6$ characterized his three dimensional disk instability models with radiative transfer that resulted in clump formation.

More recently, Meru & Bate (2010) have performed a detailed study of the effects of β on disk models with varied surface density and temperature profiles, disk masses and radii, and stellar masses, finding that a single critical value of β_{crit} is not always able to predict whether or not fragmentation occurs. In a similar vein, a recent analysis by Nero & Bjorkman (2009) found that their analytical cooling time estimates were over an order of magnitude shorter than those calculated by Rafikov (2005), and hence considerably more supportive of fragmentation. A similar conclusion was found by Boss (2005).

Here we completely avoid the debate over β_{crit} by directly calculating disk cooling through the inclusion of radiative transfer. We then use this brute force approach to attack the other pre-condition for a disk instability leading to fragmentation, namely the disk

mass.

Recent observations of low- and intermediate-mass pre-main-sequence stars imply that their disks form with masses in the range from 0.05 $M_\odot$ to 0.4 $M_\odot$ (Isella, Carpenter, & Sargent 2009). These observed disk masses form one of the primary constraints on disk instability models. Previous disk instability models by Boss (2002) for solar-mass protostars assumed disk masses of 0.091 $M_\odot$ from 4 to 20 AU, while those by Mayer et al. (2004) had disk masses ranging from 0.075 to 0.125 $M_\odot$ inside 20 AU. We present new results here for even lower mass protoplanetary disks (0.043 $M_\odot$), to learn if the disk instability mechanism for giant planet formation can continue to operate in such a low mass disk around a solar-mass protostar.

2. Numerical Methods

The calculations were performed with a numerical code that solves the three dimensional equations of hydrodynamics, including the energy equation, along with radiative transfer in the diffusion approximation and Poisson's equation for the gravitational potential. Compressional heating and radiative cooling are thus included. The same basic code has been used in all of the author's previous studies of disk instability. The code is second-order-accurate in both space and time. A complete description of the code and of the numerous tests it passed during its development may be found in Boss & Myhill (1992). More recently, the radiative transfer solution technique has been shown to be highly accurate in relaxing to, and maintaining, analytical solutions for the temperature and radiative flux profiles for both spheres and disks of gas (Boss 2009). Both the Jeans length (e.g., Boss et al. 2000) and the Toomre length (Nelson 2006) criteria are monitored throughout the runs to ensure that any clumps that might form are not numerical artifacts.

3. Initial Conditions

The disks initially have the density distribution (Boss 1993) of an adiabatic, self-gravitating, thick disk in near-Keplerian rotation about a stellar mass M_s

$$\rho(R,Z)^{\gamma-1} = \rho_o(R)^{\gamma-1} - \Big(\frac{\gamma-1}{\gamma}\Big)\Big[\Big(\frac{2\pi G\sigma(R)}{K}\Big)Z + \frac{GM_s}{K}\Big(\frac{1}{R} - \frac{1}{(R^2+Z^2)^{1/2}}\Big)\Big],$$

where R and Z are cylindrical coordinates, $\rho_o(R)$ is the midplane density, and $\sigma(R)$ is the

surface density. The adiabatic constant is $K = 1.7 \times 10^{17}$ (cgs units) and $\gamma = 5/3$ for the initial model; thereafter, the disk evolves in a nonisothermal manner governed by the energy equation and radiative transfer (Boss & Myhill 1992). The radial variation of the initial midplane density is a power law that ensures near-Keplerian rotation throughout the disk: $\rho_o(R) = \rho_{o4}(R_4/R)^{3/2}$, where $\rho_{o4} = 5 \times 10^{-11}$ g cm^{-3}, and $R_4 = 4$ AU. The surface density used to define the density distribution is: $\sigma(R) = \sigma_4(R_4/R)^{1/2}$, where $\sigma_4 = 10^3$ g cm^{-2}. The use of this analytical surface density in the above density distribution results in an initial disk surface density distribution with $\sigma \propto r^{-1/2}$ to r^{-1} in the inner disk, steepening to $r^{-3/2}$ in the outer disk (Boss 2002). Regions where the disk density falls to small values are considered to be in the infalling envelope with a density $\rho_e(R) = \rho_{e4}(R_4/R)^{3/2}$, where $\rho_{e4} = 10^{-14}$ g cm^{-3}. With $M_s = 1 M_\odot$, the disk mass is $M_d = 0.043 M_\odot$ from 4 to 20 AU, a mass roughly half that of the otherwise identical disk models in Boss (2002).

Four different models have been computed with the above disk density distribution and with different combinations of outer disk temperature T_o (20 and 25 K) and envelope temperature T_e (30 and 50 K). Model A had $T_o = 20$ K and $T_e = 50$ K, model B had $T_o = 25$ K and $T_e = 50$ K, model C had $T_o = 20$ K and $T_e = 30$ K, and model D had $T_o = 25$ K and $T_e = 30$ K. The initial disk temperatures inside 7 AU are those computed by Boss (1996) for this disk density distribution, yielding a midplane temperature of $T_m = 339$ K at 4 AU and decreasing monotonically to $T_m = 100$ K at 7 AU; thereafter, T_m is assumed to decrease smoothly to $T_o = 20$ or 25 K. [In order to err on the side of stability, the temperature is not allowed to drop below this initial distribution.] These choices lead to initial Toomre (1964) Q gravitational stability criteria decreasing monotonically outwards from values greater than 10 inside 5 AU to minimum Q values $Q_{min} = 1.74$ for models A and C and 1.95 for models B and D at the outer grid boundary of 20 AU. Higher initial Q values are expected to stifle disk fragmentation, so models B and D are intended to test the robustness of any fragmentation obtained in models A and C.

4. Results

All four models were run initially with $N_r = 100$, $N_\theta = 45$ (effectively), $N_\phi = 256$ and $N_{Ylm} = 32$ for about 100 yr of evolution. During this time period, all four models evolved in a similar manner, forming multiple trailing spiral arms that interacted with each other. The spiral arms formed throughout the disks, but were most pronounced inside ~ 10 AU. In models A and C, the spiral arm interactions would occasionally lead to the formation of transient clumps. However, analysis of these clumps did not reveal any that were massive enough to be considered self-gravitating and hence candidates for possible giant planet for-

mation. In models B and D, the spiral arms that formed were not as vigorous as those in models A and C, as expected given their slightly higher initial outer disk temperatures, and again self-gravitating clumps did not occur.

After this initial phase of evolution, all four models were doubled in their ϕ grid resolution and run further with $N_\phi = 512$ and $N_{Ylm} = 48$, effectively quadrupling the computational load by doubling the number of grid points while halving the time step. In order to maintain numerical stability for the energy equation solution, the time steps used were always small fractions of the maximum permissible explicit time differencing time step (Δt_{CFL}), often as small as 0.01 Δt_{CFL}. This resulted in painfully slow execution of the models, each of which required approximately three years of continuous processing on a dedicated Carnegie Alpha Cluster node.

Figure 1 shows the equatorial density distribution of model A after 129 yr of evolution. Strong spiral arms are apparent from the inner boundary at 4 AU out to $\sim$ 10 AU, as well as a number of clumps, often still aligned with their parental spiral arms. Figure 2 depicts the midplane temperature distribution, which rises rapidly inside $\sim$ 7 AU to a maximum of $\sim$ 340 K at 4 AU. Comparison of Figures 1 and 2 shows that the clumps form in the region most advantageous for their formation: just outside $\sim$ 7 AU, where the disk midplane temperatures begin to moderate, yet as close to the center as possible, where the orbital periods are shortest, as expected for a dynamical instability linked to the rotation period.

For model A at 129 yr, the maximum midplane density of 5.5×10^{-10} g cm^{-3} occurs for the clump seen at about 6 o'clock in Figure 1. Figure 3 presents the midplane density and temperature as a function of disk radius for an azimuthal profile that passes through the clump at $\sim$ 6 o'clock in Figure 1. Figure 3 shows that the maximum density occurs at a radius of $\sim$ 8 AU, just at the radius where the temperature profile begins to rise rapidly inward. The mass of the clump at this time is $\sim 0.26 M_J$, slightly above the Jeans mass of $\sim 0.24 M_J$ at the mean density (1.1×10^{-10} g cm^{-3}) and mean temperature (26 K) of the clump. This mass estimate implies that the clump is self-gravitating and could be expected to contract to higher densities if permitted by the spatial resolution of the grid. At the radial distance of the model A clump (7 AU), Q has dropped from an initial value of 2.7 to 1.9, allowing marginal clump formation. The tidal radius for the clump is 0.34 AU, similar to the radial half-extent of the clump seen in Figure 3. Note from Figure 3 that at this early phase, the clump has not begun to undergo any significant self-heating due to contraction. Upward convective-like motions are present in model A, but their vigor may not be sufficient to permit cooling on an orbital timescale, compared to disk models with twice the disk mass, i.e., model HR of Boss (2004). Boss (2004) estimated an effective global value of $\beta \sim 6$ for model HR; the reduced convective-like motions in model A imply a value of $\beta > 6$.

The clump orbits on a trajectory equivalent to a Keplerian orbit with a semimajor axis of 7.3 AU and an eccentricity of 0.05. The 6 o'clock clump shown in Figures 1, 2, and 3 first appeared roughly 1/4 of an orbital rotation earlier, and persists for another $\sim 1/2$ orbital rotation before the calculation was ended after a total of 143 yr of evolution (143 yr equals ~ 19 inner orbital rotation periods, as the disk's orbital rotation period is 7.7 yr at 4 AU). At that final time, the estimated clump mass had increased slightly to $\sim 0.35 M_J$, again above the Jeans mass of $\sim 0.23 M_J$ at the mean density (1.7×10^{-10} g cm^{-3}) and the slightly higher mean temperature (30 K) of the clump. This suggests that a protoplanet with an initial mass of at least $\sim 0.35 M_J$ should form from this clump. The clump's orbital eccentricity has increased to 0.09 by this time, while its semimajor axis has decreased to 6.8 AU.

A second distinct clump seen at about 10 o'clock in Figure 1 is not likely to form a protoplanet, however. At a time of 129 yr, the clump's estimated mass is $\sim 0.55 M_J$, well below its Jeans mass of $\sim 0.75 M_J$ at this mean density (6.0×10^{-11} g cm^{-3}) and mean temperature (46 K). The other clumps evident in Figure 1 suffer from the same fate of not being massive enough to be self-gravitating. Hence model A seems able to lead to only a single giant protoplanet.

Figure 4 and 5 present the midplane densities and temperatures for model B after 119 yr of evolution. Figures 4 and 5 are similar to Figures 1 and 2, although the spiral arms are not quite as robust in model B as in model A, as seen in either the density distributions of Figures 1 and 4 or the temperature distributions of Figures 2 and 5.

The most promising clump in model B at 119 yr occurs at 5 o'clock in Figures 4 and 5. The estimated clump mass is $\sim 0.21 M_J$, below the Jeans mass of $\sim 0.35 M_J$ at the mean density (1.9×10^{-10} g cm^{-3}) and mean temperature (40 K) of the clump. The clump at 7 o'clock in Figures 4 and 5 suffers from the same problem; model B appears to be close to, but not quite capable of forming self-gravitating clumps.

Models C and D are identical to models A and B except for having envelope temperatures of 30 K instead of 50 K. While the envelope temperature has some effect on the outcome of the evolutions, after 137 yr model C was only able to form a single self-gravitating clump with a mass of $\sim 0.38 M_J$ and another clump that did not exceed the Jeans mass, as was the case for model A. Similar to model B, model D was unable to form a single self-gravitating clump after 113 yr of evolution.

5. Discussion

The four models clearly show that low mass disks orbiting solar-mass protostars are less able to form self-gravitating clumps that might go on to form giant protoplanets than more massive disks. Boss (2002) presented a suite of solar-mass protostar models with disk masses of $0.091 M_{\odot}$ that are otherwise much the same as the present models, with the exception of starting their evolutions with outer disk temperatures ranging from 20 K to 50 K, resulting in initial minimum Toomre Q values ranging from 0.94 to 1.5. All of these Boss (2002) disk models formed multiple self-gravitating clumps (see, e.g., Figure 3 of Boss 2002). The present models thus suggest that the ability of disk instability to form self-gravitating clumps is severely compromised as the disk mass is lowered to $\sim 0.043 M_{\odot}$.

The results are consistent with those obtained by Mayer et al. (2007), who studied disks extending from 4 to 20 AU in orbit around a solar-mass protostar using an SPH code with diffusion approximation radiative transfer. Mayer et al. (2007) found that when the disk mass was taken to be $0.05 M_{\odot}$, the Toomre Q was below 2 in the outer disk and strong spiral arms appeared. However, fragmentation occurred in some of their models only when the disk mass was increased to $0.1 - 0.15 M_{\odot}$, with fragmentation depending on their choice of the mean molecular weight of the disk gas and of the ability to cool from the surface of the disk. Given that the Mayer et al. (2007) disks were assumed to have outer disk temperatures of 40 K, considerably warmer than the values of 20 K and 25 K studied here, the requirement of a disk mass higher than $0.05 M_{\odot}$ for fragmentation to occur in their models is consistent with the present models, as well as with those of Boss (2002), where fragmentation occurred in similar models with disk masses of $0.091 M_{\odot}$ and outer disk temperatures as high as 50 K.

While envelope temperatures of 30 to 50 K appear to reasonable bounds for a solar-mass protostar during quiescent periods (Chick & Cassen 1997), the primary question arising from these four models is what is the proper outer disk temperature? Is $T_o = 20$ K or 25 K beyond ~ 7 AU a realistic assumption? D'Alessio et al. (2006) presented T Tauri disk models with midplane temperatures of ~ 30 to 40 K at 10 AU, depending on the dust grain population. Observations of the DM Tau outer disk, on scales though of 50 to 60 AU, imply midplane temperatures of 13 to 20 K (Dartois, Dutrey, & Guilloteau 2003). Observations of cometary ices imply disk temperatures of ~ 28 K at their formation locations (Kawakita et al. 2001). The composition of the giant planets suggests that solids formed at 5.2 AU and beyond at temperatures of no more than 30 to 40 K (Owens & Encrenaz 2006). The present models suggest that outer disk temperatures must be as low as ~ 20 K in order for disk instability to have a chance to form giant protoplanets in these relatively low mass disks, and it is unclear at present if such low outer disk temperatures are realistic or not.

6. Conclusions

Boss (2002) found that robust disk instablities could occur inside 20 AU in disks with a mass of $\sim 0.091 M_{\odot}$. The present models show that when the disk mass inside 20 AU is halved, the ability of disk instability to produce viable, self-gravitating clumps is signficantly compromised, when self-consistently-calculated disk cooling rates are employed. Disk instability thus appears to be only a marginally effective process in a disk with $\sim 0.04 M_{\odot}$, and is unlikely to lead to giant planet formation around solar-mass protostars with disks significantly less massive than $\sim 0.04 M_{\odot}$. Clearly core accretion remains as the favored formation mechanism for giant planets in such lower mass disks.

I thank the referee for a number of perceptive comments, Sandy Keiser for computer systems support and John Chambers for advice on orbit determinations. This research was supported in part by NASA Planetary Geology and Geophysics grant NNX07AP46G, and is contributed in part to NASA Astrobiology Institute grant NNA09DA81A. The calculations were performed on the Carnegie Alpha Cluster, the purchase of which was partially supported by NSF Major Research Instrumentation grant MRI-9976645.

REFERENCES

Boley, A. C. 2009, ApJ, 695, L53

Boss, A. P. 1993, ApJ, 417, 351

——. 1996, ApJ, 469, 906

——. 2002, ApJ, 576, 462

——. 2004, ApJ, 610, 456

——. 2005, ApJ, 629, 535

——. 2009, ApJ, 694, 107

——. 2010, ApJ, submitted

Boss, A. P., & Myhill, E. A. 1992, ApJS, 83, 311

Boss, A. P., Fisher, R. T., Klein, R. I., & McKee, C. F. 2000, ApJ, 528, 325

Chambers, J. E. 2006, ApJL, 652, L133

Chick, K. M., & Cassen, P. 1997, ApJ, 477, 398

Cumming, A., et al. 2008, PASP, 120, 531

D'Alessio, P., et al. 2006, ApJ, 638, 314

Dartois, E., Dutrey, A., & Guilloteau, S. 2003, A&A, 399, 773

Dodson-Robinson, S. E., Veras, D., Ford, E. B., & Beichman, C. A. 2009, ApJ, 707, 79

Gammie, C. F. 2001, ApJ, 553, 174

Gould, A. et al. 2010, ApJ, 720, 1073

Helled, R., Podolak, M., & Kovetz, A. 2006, Icarus, 185, 64

Helled, R., & Bodenheimer, P. 2010, Icarus, submitted

Isella, A., Carpenter, J. M., & Sargent, A. I. 2009, ApJ, 701, 260

Johnson, J. A., Aller, K. M., Howard, A. W., & Crepp, J. R. 2010, PASP, 122, 905

Kawakita, H., et al. 2001, Science, 294, 1089

Levison, H. F., & Stewart, G. R. 2001, Icarus, 153, 224

Marois, C., et al. 2008, Science, 322, 1348

Mayer, L., Lufkin, G., Quinn, T., & Wadsley, J. 2007, ApJ, 661, L77

Mayer, L., Quinn, T., Wadsley, J., & Stadel, J. 2004, ApJ, 609, 1045

Mayor, M., et al. 2009, A&A, 507, 487

Meru, F., & Bate, M. R. 2010, MNRAS, in press

Nelson, A. F. 2006, MNRAS, 373, 1039

Nero, D., & Bjorkman, J. E. 2009, ApJ, 702, L163

Owens, T., & Encrenaz, T. 2006, Planet. Space Sci., 54, 1188

Rafikov, R. R. 2005, ApJ, 621, L69

Raymond, S. N., Armitage, P. J., & Gorelick, N. 2010, ApJ, 711, 772

Rice, W. K. M., Armitage, P. J., Bate, M. R., & Bonnell, I. A. 2003, MNRAS, 339, 1025

Thommes, E. W., Duncan, M. J., & Levison, H. F. 2002, AJ, 123, 2862

Toomre, A. 1964, ApJ, 139, 1217

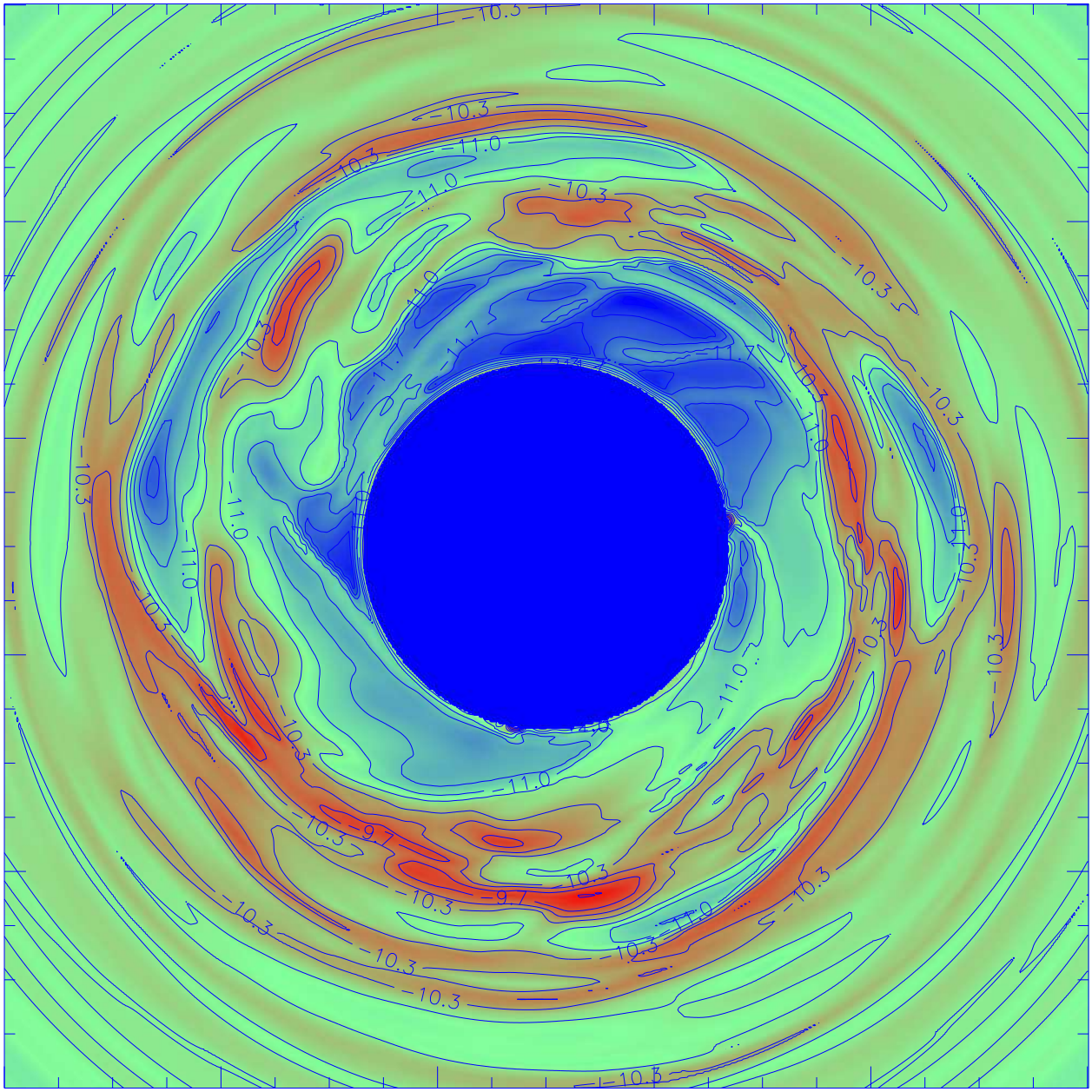

Fig. 1.— Equatorial log density for model A after 129 yr of evolution. Colors span a rainbow running from blue (low density) to red (high density). Contours are spaced by factors of ~ 2 in density. Region shown is 24 AU wide; inner region (blue) is 4 AU in radius.

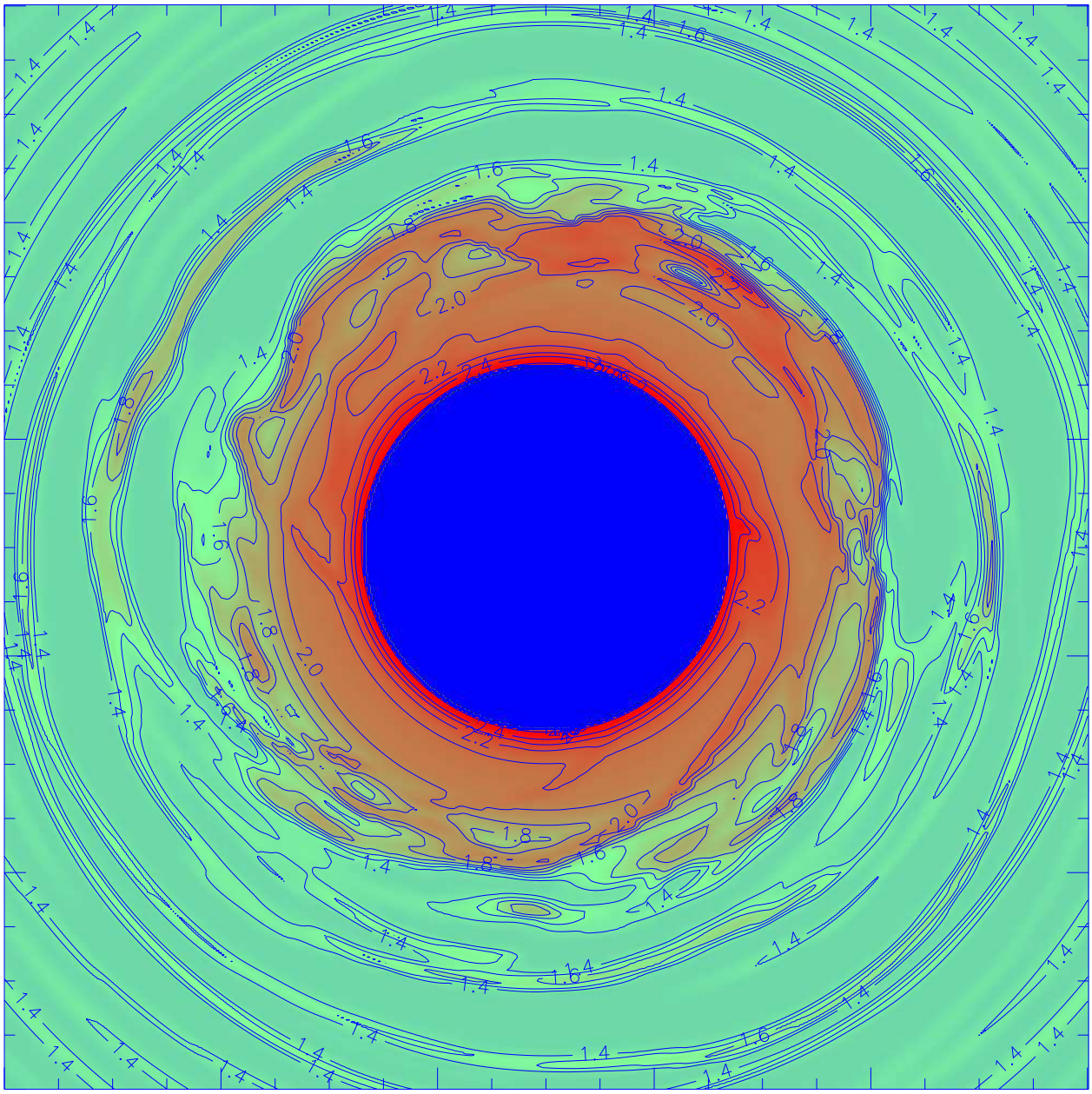

Fig. 2.— Equatorial log temperature for model A after 129 yr of evolution, plotted as in Figure 1, except that the contours are spaced by factors of ~ 1.3 in temperature.

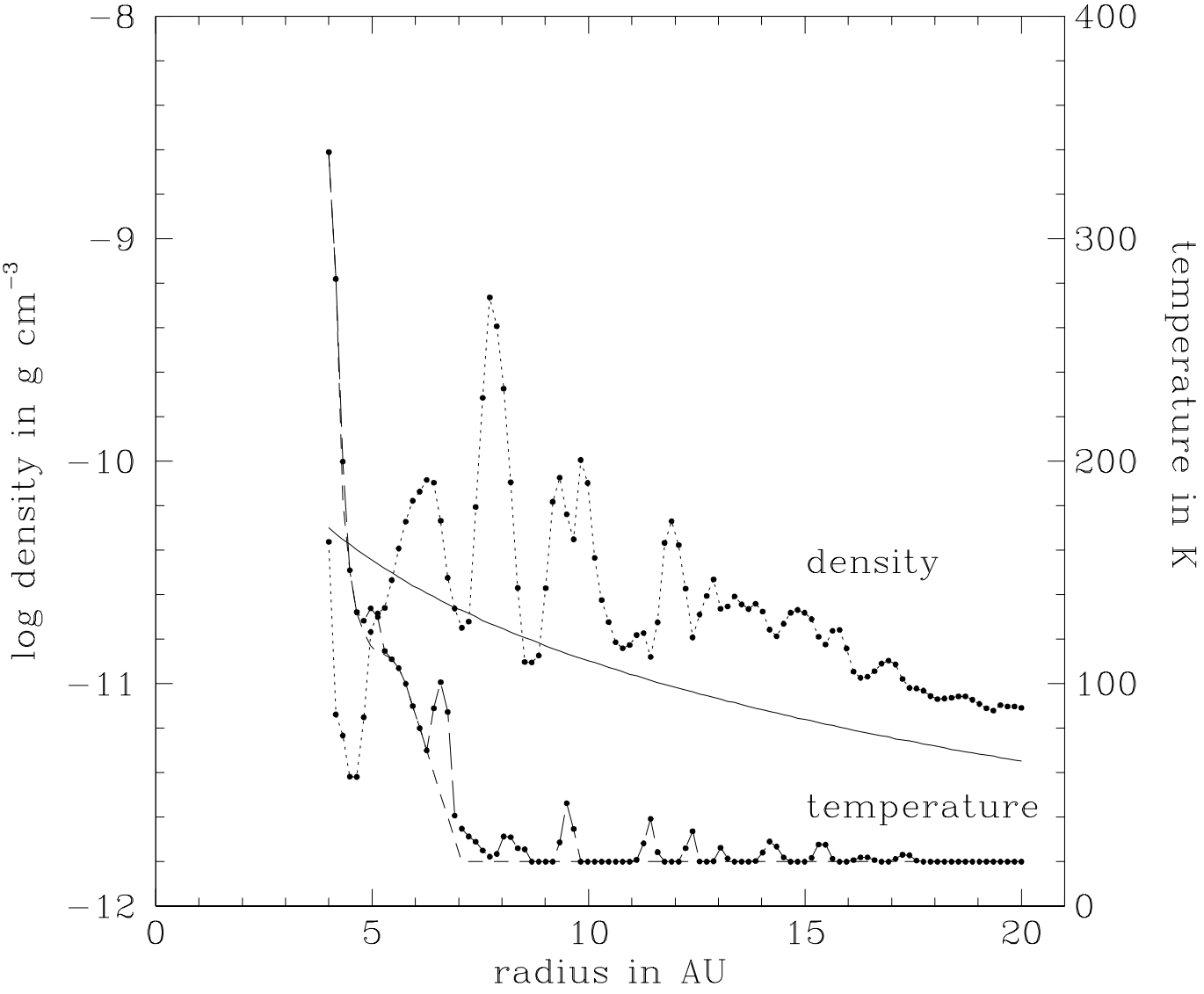

Fig. 3.— Initial log density (solid line) and temperature (dashed line) for model A, as well as after 129 yr of evolution (points), for an azimuthal profile in the equatorial plane that passes through the clump in Figure 1 at $\sim$ 6 o'clock.

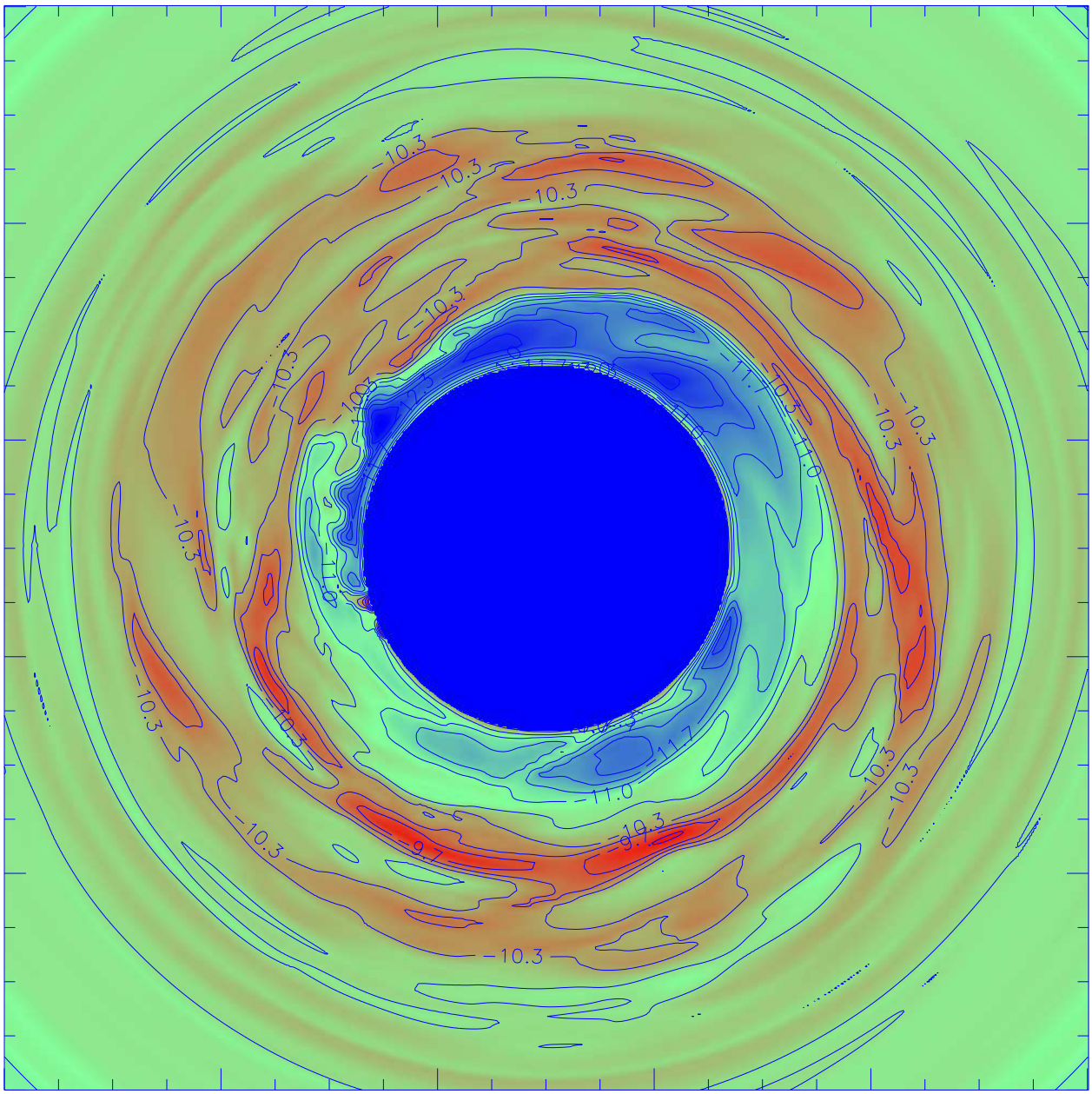

Fig. 4.— Equatorial log density for model B after 119 yr of evolution, plotted as in Figure 1.

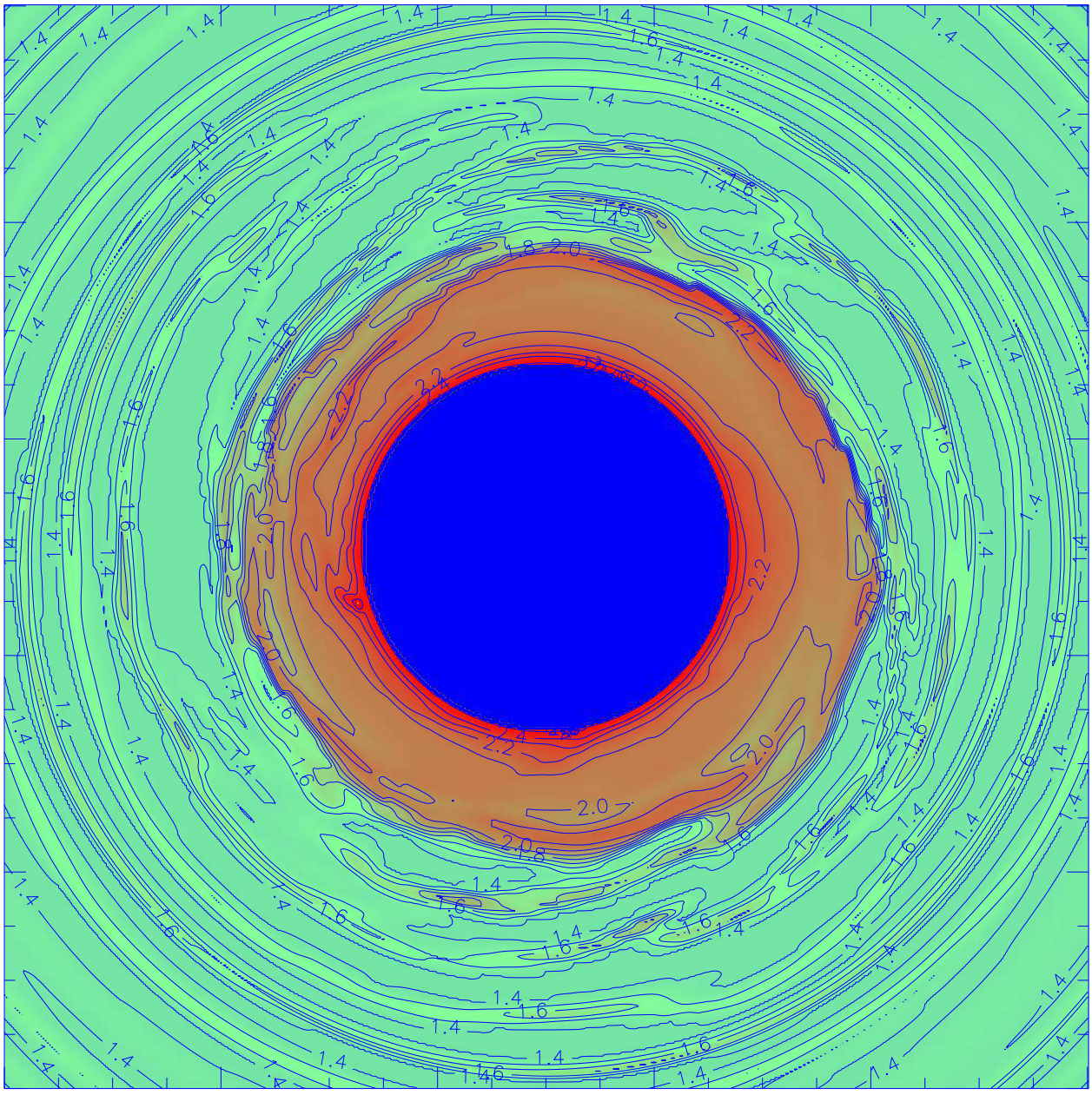

Fig. 5.— Equatorial log temperature for model B after 119 yr of evolution, plotted as in Figure 2.